

Low Field Nano-NMR via Three-Level System Control

J. Cerrillo^{1,*}, S. Oviedo Casado², and J. Prior^{3,1,4}

¹*Área de Física Aplicada, Universidad Politécnica de Cartagena, Cartagena E-30202, Spain*

²*Racah Institute of Physics, The Hebrew University of Jerusalem, Jerusalem 91904, Givat Ram, Israel*

³*Departamento de Física-CIOyN, Universidad de Murcia, Murcia E-30071, Spain*

⁴*Instituto Carlos I de Física teórica y Computacional, Universidad de Granada, Granada E-18071, Spain*



(Received 6 October 2020; accepted 20 April 2021; published 3 June 2021)

Conventional control strategies for nitrogen-vacancy centers in quantum sensing are based on a two-level model of their triplet ground state. However, this approach fails in regimes of weak bias magnetic fields or strong microwave pulses, as we demonstrate. To overcome this limitation, we propose a novel control sequence that exploits all three levels by addressing a hidden Raman configuration with microwave pulses tuned to the zero-field transition. We report excellent performance in typical dynamical decoupling sequences, opening up the possibility for nano-NMR operation in low field environments.

DOI: [10.1103/PhysRevLett.126.220402](https://doi.org/10.1103/PhysRevLett.126.220402)

Paramagnetic defects in diamonds feature prominently in magnetometry oriented quantum sensing. The most widely used of these defects is the electronic spin of a negatively charged nitrogen-vacancy (NV) center [1–3], whose ground state can be described in terms of a spin-1 triplet endowed with a surprisingly long coherence time even at ambient conditions [4–7]. Its unique properties make of the NV center a remarkable sensor of the minute magnetic fields created by nanosized samples [8–13]. The NV has positioned itself as the leader in the race to achieve the ultimate nuclear magnetic resonance (NMR) spectrometer, in which a spin probe measures the magnetic field created by a distant single spin [14–17]. As well, a superior ability to measure other physical magnitudes such as temperature or electric fields has been demonstrated [18,19]. The success of NV centers as quantum sensors is based on the ability to control the spin probe and extend the duration of its coherence beyond the correlation time of the measured oscillating signal.

Typically, the NV center is considered as a two level system (2LS) thanks to the Zeeman splitting of the $|\pm 1\rangle$ levels that is introduced by means of a bias magnetic field aligned with the NV axis. Most control protocols involve dynamical decoupling (DD) sequences of microwave pulses resonant with the $|0\rangle \leftrightarrow |-1\rangle$ transition [20–34], as indicated by the red arrow in Fig. 1(a). These protocols conventionally make use of the assumption that pulses are negligibly short (impulsive limit). This actually poses a problem since, in order to conserve the pulse area, the intensity must compensate for the reduced duration. When the intensity becomes comparable to the Zeeman splitting, the 2LS approximation fails [35], resulting in a degradation of coherence time and sensitivity. Nevertheless, working in the regime of very low Zeeman splitting ($\lesssim 20$ G) becomes

necessary for ultra-low field detection or environment quantum control [17,36–41].

In this Letter, we propose an alternative route to high precision low field quantum sensing through three-level system (3LS) techniques [42,43]. Rather than struggling with the 2LS approximation we utilize a different DD frequency which addresses equally all of the NV ground spin triplet states, as depicted in Fig. 1. This allows high precision measurements at low Zeeman splitting or, equivalently, permits the use of high-power pulses, consequently providing a much wider sensitivity range. Previous works involving the $|+1\rangle$ spin state have already demonstrated fourfold enhanced sensitivity thanks to the double quantum transition $|-1\rangle \leftrightarrow |+1\rangle$ [37,44–46]. However, these proposals still rely, just as conventional methods, on the 2LS approximation, which brings back the problem of state overlap at low bias field. Instead, by addressing both $|\pm 1\rangle$ states with the same pulse, our proposal manages accurate 3LS control with stark robustness to pulse errors, thus providing high fidelity in a regime so far lacking appropriate control protocols.

Moreover, we tackle the effect of the finite length T of the pulses. This has previously been considered in the context of DD sequences, demonstrating that the finite temporal width of the pulses is crucial to calculate the optimal phase acquisition time and to match the spin precession with the signal frequency [47,48]. Nonetheless, these approaches focus on 2LSs and assume complete suppression of the signal whenever the pulse is acting, ignoring that some phase is indeed gathered during that time. Instead, we provide an improved analytical approach and full numerical calculations.

The combination of a Raman control strategy [42] for NV centers together with the consideration of finite duration of

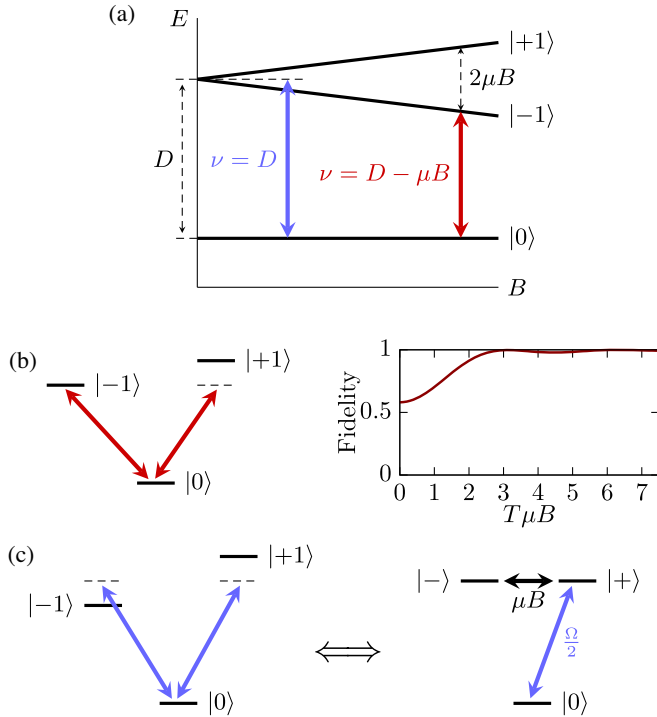


FIG. 1. (a) The ground state manifold of the NV is a spin-1 triplet where the $|\pm 1\rangle$ states are degenerate and separated from the state $|0\rangle$ by a zero field splitting of $D = 2.87$ GHz. A static magnetic field produces further splitting of the $|\pm 1\rangle$ states and allows to work with a quasi-2LS, via DD sequences of frequency matching the $|0\rangle \rightarrow |-1\rangle$ gap (red arrow). We propose instead addressing the whole 3LS with a DD frequency $\nu = D$ (blue arrow). (b) Fidelity of state $(|-1\rangle + i|0\rangle)/\sqrt{2}$ after a microwave $\pi/2$ pulse of duration T applied on an NV center initialized in state $|0\rangle$, represented as a function of the dimensionless quantity $T\mu B$. At small Zeeman splittings or short pulse lengths, poor fidelities are achieved due to off-resonant excitation of the state $|+1\rangle$. (c) By driving the system at $\nu = D$, an effective Raman coupling is implemented, providing accurate control of the system even at large intensities or low bias fields.

pulses opens up the possibility of highly precise weak measurements in low field nanoscale NMR.

Conventional control strategy.—We consider an NV center under the effect of an external, bias magnetic field in the z direction $\mathbf{B} = (0, 0, B)$ and controlled with a microwave field of frequency ν . The corresponding Hamiltonian is

$$H(\nu) = DS_z^2 + \mu BS_z + \Omega \cos \nu t S_x, \quad (1)$$

where D is the zero field splitting, μ is the gyromagnetic ratio of electrons, Ω is the Rabi frequency associated with the microwave drive, and S_j is the spin-1 Pauli matrix in the j th direction. The dependence of the eigenvalues with the strength of the magnetic field B is depicted in Fig. 1(a).

Control of the NV center is usually achieved by setting $\nu = D - \mu B$ [red coupling in Fig. 1(a)]. We will refer to this

strategy as the conventional control (CC) scheme. At this frequency, the microwave field spectrally addresses the $|0\rangle \leftrightarrow |-1\rangle$ transition, as revealed by the Hamiltonian in the appropriate rotating picture

$$\begin{aligned} \tilde{H}(D - \mu B) &\simeq 2\mu B | +1\rangle \langle +1| \\ &+ \frac{\Omega}{2\sqrt{2}} (|-1\rangle \langle 0| + |+1\rangle \langle 0| + \text{H.c.}). \end{aligned} \quad (2)$$

Because of the existence of a matrix element $\langle 0|S_x|+1\rangle$, the 2LS approximation remains valid only as long as transitions to the state $|+1\rangle$ can be neglected, either because the bias field B sets it sufficiently apart or because the microwave intensity Ω is weak enough. Beyond this regime, pulse control becomes imprecise and fails to perform the expected task, as illustrated in Fig. 1(b) for the case of a $\pi/2$ pulse of duration $T = \pi/(\sqrt{2}\Omega)$. There, we represent the fidelity of the target state $(|-1\rangle + i|0\rangle)/\sqrt{2}$ as a function of the dimensionless product $T\mu B$. The target state becomes depleted by off-resonant excitation to $|+1\rangle$ either as the Zeeman splitting is reduced or as the pulse intensity increases. Therefore, the ideal of the impulsive limit is actually not desirable in this context and it is always necessary to resort to finite pulse lengths.

Proposed control strategy.— In order to avoid the detrimental effect illustrated in Fig. 1(b), we propose the effective Raman control (NV-ERC) strategy, which involves both the $|-1\rangle$ and $|+1\rangle$ states by setting the microwave frequency rather to $\nu = D$ [blue coupling in Fig. 1(a)]. In the absence of noise sources, a coherent superposition with fidelity 1 is possible at this spectral position even in the limit of high intensity pulses or small Zeeman splitting (for the effect of microwave source noise see Supplemental Material [49]). This is due to the hidden effective Raman coupling

$$\tilde{H}(D) \simeq \left(\mu B |- \rangle + \frac{\Omega}{2} |0\rangle \right) \langle + | + \text{H.c.}, \quad (3)$$

revealed by the basis $|\pm\rangle = (|+1\rangle \pm |-1\rangle)/\sqrt{2}$ [see Fig. 1(c)]. This Hamiltonian produces Rabi oscillations of frequency $\bar{\Omega} = \sqrt{\mu^2 B^2 + \Omega^2/4}$ and period $\bar{T} = 2\pi/\bar{\Omega}$ between states $|+\rangle$ and $[\mu B |- \rangle + (\Omega/2)|0\rangle]/\bar{\Omega}$.

With this structure, it is possible to improve the two types of pulses required in most DD sequences. For the population to coherence map (commonly a $\pi/2$ pulse of length T), we introduce the notion of a pulse of strength $\Omega \geq 2\mu B$ applied for a time

$$\bar{T}' = \frac{\arccos\left(-\frac{4\mu^2 B^2}{\Omega^2}\right)}{\bar{\Omega}}, \quad (4)$$

which transforms $|0\rangle$ into $|\phi\rangle = [|-1\rangle - \exp(i\phi)|+1\rangle]/\sqrt{2}$ with $\cos \phi = (8\mu^2 B^2/\Omega^2) - 1$. The opposite transformation $|\phi\rangle \rightarrow |0\rangle$ is achieved in the time remaining off the Rabi

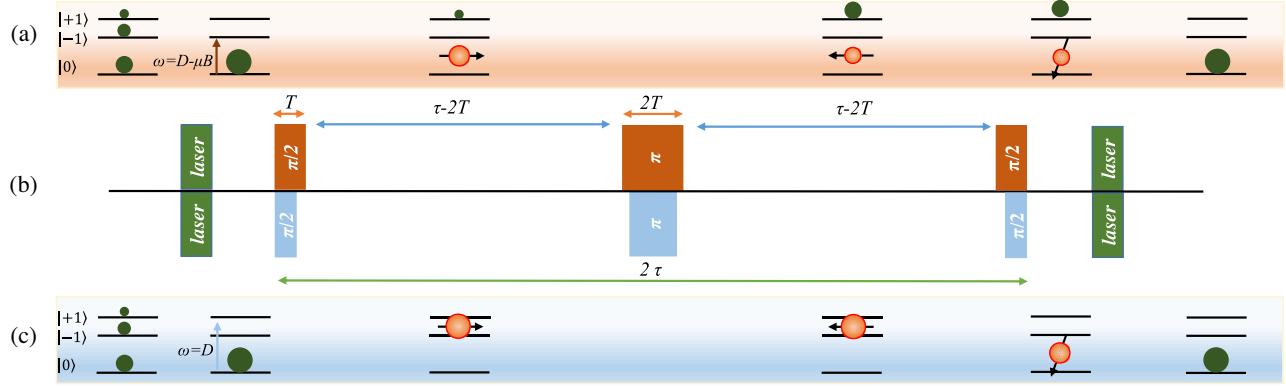


FIG. 2. *Protocol.*—Depiction of a DD protocol for magnetometry with NV centers and comparison between CC and NV-ERC. In (a), the usual DD sequence [upper (b)] creates an initial superposition $|0\rangle + |-1\rangle$, but additionally partially populates the $|+1\rangle$ state. Pulses have to be lengthened in order to ensure a high fidelity truer to the 2LS framework. As a consequence, sensitivity is limited. In (c) on the contrary, the pulses address the three levels and create a coherent superposition $|+1\rangle + |-1\rangle$ without contamination from the $|0\rangle$ state. This permits reducing the duration of the pulses in our proposed DD sequence [lower (b)], which increases sensitivity for the same total duration, or permits introducing more pulses within the same DD sequence, without loss of signal and working at low bias field.

period $\tilde{T}'' = \tilde{T} - \tilde{T}'$. Unlike the pulses discussed above, these remain exact for increasing Ω .

The Bloch sphere rotation (usually a π pulse of length $2T$) is implemented by a 2π pulse with $\Omega \gg \mu B$ of length $T' = 2\sqrt{2}T$, which produces the phase gate $|+\rangle \rightarrow -|+\rangle$. This pulse improves its performance as the impulsive limit is approached, also in stark contrast to the case described above.

Application in DD sequences.— A schematic representation and comparison of both CC and NV-ERC strategies in the context of a Hahn-echo sequence is illustrated in Fig. 2. Both pulse sequences are represented in Fig. 2(b). Additionally, the effects in the state of the 3LS are represented in Fig. 2(a) for CC and Fig. 2(c) for NV-ERC. There, coherences between levels are represented by orange Bloch spheres and their corresponding vectors, while residual population is represented by green spheres of varying diameters. Starting with a thermal distribution of population across the three states, a laser pulse first initializes the NV at $|0\rangle$. A microwave $\pi/2$ pulse of length T (\tilde{T}') then attempts to generate an equal superposition of the two states $|0\rangle$ and $|-1\rangle$ ($|+1\rangle$ and $|-1\rangle$). An unwanted population appears at $|+1\rangle$ in Fig. 2(a), whereas this problem is avoided in Fig. 2(c). After a free evolution time $\tau - 2T$ ($\tau - T'/2 - \tilde{T}/2$), where 2τ is the total time of the sequence, a π pulse of length $2T$ (T') is applied to invert the Bloch sphere in the respective 2LS. Following an equal free evolution time, another $\pi/2$ pulse of duration T (\tilde{T}'') aims at converting coherences to populations, which are finally measured by a laser pulse (which also reinitializes the NV center). Each microwave pulse in Fig. 2(a) accumulates additional population in $|+1\rangle$, rendering the sequence increasingly imprecise.

Ramsey sequence.—To compare both strategies, we resort to the concept of the filter function (FF) $F(\omega) = f_r^2(\omega) + f_i^2(\omega)$. For a coherent external field perturbation $\mathbf{B}'_r(\omega) = \cos(\omega t)(0, 0, 1)$ [$\mathbf{B}'_i(\omega) = \sin(\omega t)(0, 0, 1)$], $f_r(\omega)$ [$f_i(\omega)$] is equivalent to the accumulated phase in the NV [49], allowing us to directly relate analytical calculations of FFs with numerical results of the performance of each control sequence. Let us first consider the simpler case of an ideal Ramsey experiment, which involves an initial $\pi/2$ pulse, waiting time, and a final $\pi/2$ pulse. In the impulsive limit, it features the FF

$$F_R(\omega) = \tau^2 \text{sinc}^2\left(\frac{\omega\tau}{2}\right), \quad (5)$$

where τ is the total duration of the experiment and $\text{sinc}(x) = \sin(x)/x$. As expected, it peaks at vanishing frequency, confirming that this sequence is mostly sensitive to continuous noise. This function also indicates that longer experiments are preferred for two reasons. First, they yield stronger signals as indicated by the factor τ^2 . Second, longer experiments have better frequency selectivity as indicated by the sinc dependency. This is explained by the fact that only perturbations whose periods are longer than τ can be detected, while the signal associated to faster oscillations averages out.

As discussed above, the impulsive limit $T \rightarrow 0$ is not desirable in the context of NV centers. Nevertheless, a finite pulse length T has detrimental effects in the sensitivity of experiments [47,48]. This can be shown even in the context of an ideal 2LS, where an improved expression incorporating the dependency on T can be derived [49]

$$F_R(\omega, T) = (\tau - T)^2 \text{sinc}^2\left(\omega \frac{T}{2}\right) \text{sinc}^2\left(\omega \frac{\tau - T}{2}\right). \quad (6)$$

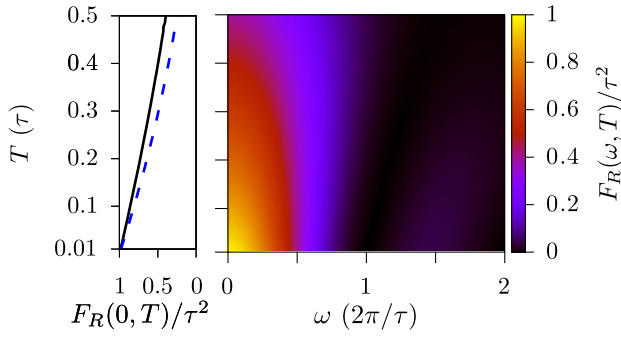


FIG. 3. Filter function $F_R(\omega, T)$ of a Ramsey experiment as a function of the $\pi/2$ -pulse duration T and the signal frequency ω in the ideal case of a 2LS. The left panel compares the values of $F_R(0, T)$ from the numerical calculation (black solid curve) and the analytical calculation Eq. (6) (blue dashed curve).

The prefactor $(\tau - T)^2$ clearly indicates that the strength of the signal is heavily diminished by T . Additionally, a slight broadening of the function takes place between the ideal limit $T = 0$ in Eq. (5) and the maximum pulse length possible $T = \tau/2$, where $F_R(\omega, \tau/2) = (\tau/2)^2 \text{sinc}^4(\omega\tau/4)$, so pulse length also reduces frequency selectivity.

Improving on Eq. (6), we perform a numerical calculation of the remaining ground state population $p_{r,i}(\omega, T)$ of a 2LS after a Ramsey sequence of total duration τ (including pulse length T) under the effect of the signal $\mathbf{B}_{r,i}'(\omega)$. Using the relation $f_{r,i} = \arccos(1 - 2p_{r,i})$ between population and accumulated phase, we can compute the associated numerical FF as shown in Fig. 3. The left panel represents the value of the FF for $\omega = 0$ as compared to the prediction of Eq. (6) $F_R(0, T) = (\tau - T)^2$. Signal loss with T is slightly overestimated by Eq. (6), but the trend is confirmed numerically as the most crucial consequence of lengthening the pulse duration. Frequency selectivity is also lost as shown by the slight broadening of the function with T , visible in the main panel.

An analogous numerical simulation has been performed for an NV center modeled by Eq. (1) and the results are shown in Fig. 4 for CC (left panel) and for NV-ERC (right panel). Accumulated contamination of $|+1\rangle$ for $T\mu B \leq 1$ utterly blurs the signal in the case of CC. Only for $T\mu B \gg 1$ a faint Ramsey profile may be recovered. In contrast, NV-ERC strongly features the profile of Eq. (5) in the regime where standard operation fails. Additionally, it provides a rather intense signal due to the double quantum separation between the involved states $|\pm 1\rangle$.

Hahn-echo sequence and beyond.—More complex DD sequences are routinely used in experiment. They amount to the introduction of N equally spaced π pulses of length $2T$. The case $N = 1$, known as the Hahn-echo experiment, is illustrated in Fig. 2. Following the analysis above, an odd amount $N = 2n + 1$ of π pulses produces a FF of the form [49]

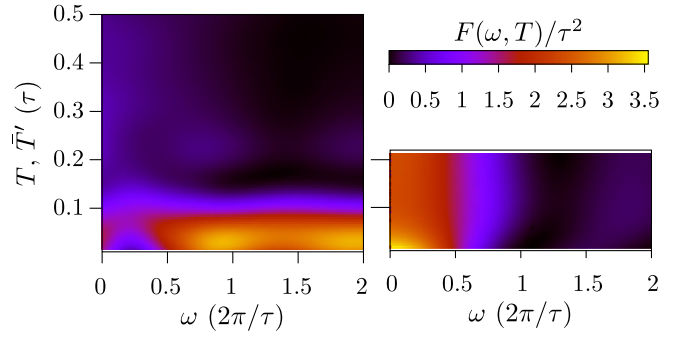


FIG. 4. Filter function $F_R(\omega, T)$ of a Ramsey experiment as a function of pulse duration and signal frequency ω for an NV center [Eq. (1)] using CC (left panel, vertical axis corresponding to T) and NV-ERC (right panel, vertical axis corresponding to \bar{T}'). The value of the Zeeman splitting is $\mu B = 10/\tau$, which imposes $\bar{T}' \leq \tau\pi/10\sqrt{2} \approx 0.22\tau$.

$$F_{2n+1}(\omega, T) = 4\sin^2\left(\omega\frac{\tau}{2}\right) \frac{\cos^2(N\omega\frac{2\tau-T}{2})}{\cos^2(\omega\frac{2\tau-T}{2})} F_R(\omega, T), \quad (7)$$

while an even amount $N = 2n > 0$ produces

$$F_{2n}(\omega, T) = 4\sin^2\left(\omega\frac{\tau}{2}\right) \frac{\sin^2(N\omega\frac{2\tau-T}{2})}{\cos^2(\omega\frac{2\tau-T}{2})} F_R(\omega, T). \quad (8)$$

The first factor centers the signal around $\omega = \pi/\tau$, whereas the second one centers it around $\omega = \pi/(\tau - T)$. The function becomes increasingly peaked around this last value for increasing N . Therefore, in addition to the effects discussed above, the pulse length T disturbs the value of the addressed frequency. This behavior is reproduced by the numerical calculation for a Hahn-echo sequence on an ideal 2LS [49]. As in Fig. 4, the same sequence on an NV center modeled by Eq. (1) fails in the region $T\mu B \leq 1$, whereas with NV-ERC the Hahn-echo profile is successfully recovered in that regime.

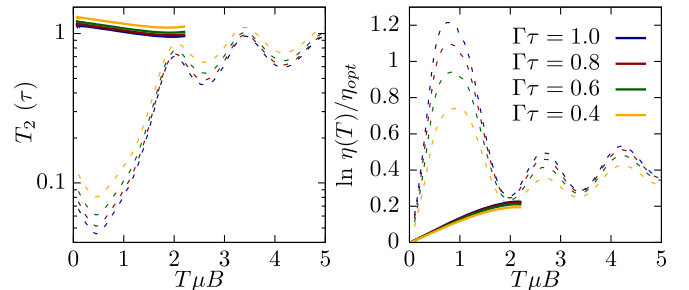


FIG. 5. Estimated coherence time T_2 (left) and sensitivity η (right) as a function of the product $T\mu B$ for CC (dashed lines) and NV-ERC (solid lines) for different widths Γ of a Lorentzian noise. Sensitivity is expressed in units of optimal sensitivity η_{opt} in the impulsive limit and without decoherence effects.

In order to illustrate this effect in the context of experimentally relevant figures of merit, in Fig. 5 we estimate the corresponding coherence times T_2 and sensitivities η [49] for both protocols in the presence of different Lorentzian environments. In the CC case, both coherence time and sensitivity are heavily degraded for small $T\mu B$, that is, in the presence of either small magnetic field or short, intense pulses. In contrast, the problem is resolved by NV-ERC in its region of applicability.

Conclusions.—Quantum sensing with arbitrary precision requires from an ever increasing sophistication of control protocols. Here, we have demonstrated that the usual paradigm that considers the NV as a two-level system fails whenever the control pulses are strong or the bias field is low. We solve the problem by exploiting a Raman configuration involving both $|\pm 1\rangle$ states, and demonstrate that with such a control technique it is possible to access the low bias field regime and at the same time recover the ideal of the impulsive limit without degradation of the signal and, consequently, without loss of sensitivity. Performing accurate experiments in this parameter region could be of interest for a number of sensing implementations, such as temperature, strain, or electric field, since it is at low bias field where these magnitudes have the greatest impact. Moreover, low frequency magnetic fields are better detected in such a way. Hence, our protocol represents a crucial extension of the nano-NMR scheme.

We thank Daniel Louzon and Alex Retzker for useful discussions. J.C. acknowledges the support from Ministerio de Ciencia, Innovación y Universidades (Spain) (“Beatriz Galindo” Fellowship BEAGAL18/00081), S.O.C. is supported by the Fundación Ramón Areces postdoctoral fellowship (XXXI edition of grants for Postgraduate Studies in Life and Matter Sciences in Foreign Universities and Research Centers), and J.P. is grateful for financial support from Ministerio de Ciencia, Innovación y Universidades (Spain) Project No. PGC2018-097328-B-I00, FEDER funds FIS2015-69512-R and Fundación Séneca (Murcia, Spain) Projects No. 19882/GERM/15.

*javier.cerrillo@upct.es

- [1] F. Jelezko, I. Popa, A. Gruber, C. Tietz, J. Wrachtrup, A. Nizovtsev, and S. Kilin, Single spin states in a defect center resolved by optical spectroscopy, *Appl. Phys. Lett.* **81**, 2160 (2002).
- [2] F. Jelezko, T. Gaebel, I. Popa, A. Gruber, and J. Wrachtrup, Observation of Coherent Oscillations in a Single Electron Spin, *Phys. Rev. Lett.* **92**, 076401 (2004).
- [3] M. W. Doherty, N. B. Manson, P. Delaney, F. Jelezko, J. Wrachtrup, and L. C. L. Hollenberg, The nitrogen-vacancy colour centre in diamond, *Phys. Rep.* **528**, 1 (2013).
- [4] L. Childress, M. V. Gurudev Dutt, J. M. Taylor, A. S. Zibrov, F. Jelezko, J. Wrachtrup, P. R. Hemmer, and M. D. Lukin, Coherent Dynamics of Coupled Electron and Nuclear Spin Qubits in Diamond, *Science* **314**, 281 (2006).
- [5] G. Balasubramanian, I. Y. Chan, R. Kolesov, M. Al-Hmoud, J. Tisler, C. Shin, C. Kim, A. Wojcik, P. R. Hemmer, A. Krueger, T. Hanke, A. Leitenstorfer, R. Bratschitsch, F. Jelezko, and J. Wrachtrup, Nanoscale imaging magnetometry with diamond spins under ambient conditions, *Nature (London)* **455**, 648 (2008).
- [6] J. R. Maze, P. L. Stanwix, J. S. Hodges, S. Hong, J. M. Taylor, P. Cappellaro, L. Jiang, M. V. Gurudev Dutt, E. Togan, A. S. Zibrov, A. Yacoby, R. L. Walsworth, and M. D. Lukin, Nanoscale magnetic sensing with an individual electronic spin in diamond, *Nature (London)* **455**, 644 (2008).
- [7] V. Jacques, P. Neumann, J. Beck, M. Markham, D. Twitchen, J. Meijer, F. Kaiser, G. Balasubramanian, F. Jelezko, and J. Wrachtrup, Dynamic Polarization of Single Nuclear Spins by Optical Pumping of Nitrogen-Vacancy Color Centers in Diamond at Room Temperature, *Phys. Rev. Lett.* **102**, 057403 (2009).
- [8] T. Staudacher, F. Shi, S. Pezzagna, J. Meijer, J. Du, C. A. Meriles, F. Reinhard, and J. Wrachtrup, Nuclear magnetic resonance spectroscopy on a (5-Nanometer)³ sample volume, *Science* **339**, 561 (2013).
- [9] H. J. Mamin, M. Kim, M. H. Sherwood, C. T. Rettner, K. Ohno, D. D. Awschalom, and D. Rugar, Nanoscale nuclear magnetic resonance with a nitrogen-vacancy spin sensor, *Science* **339**, 557 (2013).
- [10] C. Müller, X. Kong, J.-M. Cai, K. Melentijević, A. Stacey, M. Markham, D. Twitchen, J. Isoya, S. Pezzagna, J. Meijer, J. F. Du, M. B. Plenio, B. Naydenov, L. P. McGuinness, and F. Jelezko, Nuclear magnetic resonance spectroscopy with single spin sensitivity, *Nat. Commun.* **5**, 4703 (2014).
- [11] A. Ajoy, U. Bissbort, M. D. Lukin, R. L. Walsworth, and P. Cappellaro, Atomic-Scale Nuclear Spin Imaging Using Quantum-Assisted Sensors in Diamond, *Phys. Rev. X* **5**, 011001 (2015).
- [12] I. Lovchinsky, A. O. Sushkov, E. Urbach, N. P. de Leon, S. Choi, K. De Greve, R. Evans, R. Gertner, E. Bersin, C. Müller, L. McGuinness, F. Jelezko, R. L. Walsworth, H. Park, and M. D. Lukin, Nuclear magnetic resonance detection and spectroscopy of single proteins using quantum logic, *Science* **351**, 836 (2016).
- [13] D. R. Glenn, D. B. Bucher, J. Lee, M. D. Lukin, H. Park, and R. L. Walsworth, High-resolution magnetic resonance spectroscopy using a solid-state spin sensor, *Nature (London)* **555**, 351 (2018).
- [14] S. Kolkowitz, Q. P. Unterreithmeier, S. D. Bennett, and M. D. Lukin, Sensing Distant Nuclear Spins with a Single Electron Spin, *Phys. Rev. Lett.* **109**, 137601 (2012).
- [15] T. H. Taminiau, J. J. T. Wagenaar, T. van der Sar, F. Jelezko, V. V. Dobrovitski, and R. Hanson, Detection and Control of Individual Nuclear Spins Using a Weakly Coupled Electron Spin, *Phys. Rev. Lett.* **109**, 137602 (2012).
- [16] N. Zhao, J. Honert, B. Schmid, M. Klas, J. Isoya, M. Markham, D. Twitchen, F. Jelezko, R.-B. Liu, H. Fedder, and J. Wrachtrup, Sensing single remote nuclear spins, *Nat. Nanotechnol.* **7**, 657 (2012).

- [17] A. Laraoui, F. Dolde, C. Burk, F. Reinhard, J. Wrachtrup, and C. A. Meriles, High-resolution correlation spectroscopy of ^{13}C spins near a nitrogen-vacancy centre in diamond, *Nat. Commun.* **4**, 1651 (2013).
- [18] F. Dolde, H. Fedder, M. W. Doherty, T. Nöbauer, F. Rempp, G. Balasubramanian, T. Wolf, F. Reinhard, L. C. L. Hollenberg, F. Jelezko, and J. Wrachtrup, Electric-field sensing using single diamond spins, *Nat. Phys.* **7**, 459 (2011).
- [19] P. Neumann, I. Jakobi, F. Dolde, C. Burk, R. Reuter, G. Waldherr, J. Honert, T. Wolf, A. Brunner, J. H. Shim, D. Suter, H. Sumiya, J. Isoya, and J. Wrachtrup, High-precision nanoscale temperature sensing using single defects in diamond, *Nano Lett.* **13**, 2738 (2013).
- [20] A. Maudsley, Modified Carr-Purcell-Meiboom-Gill sequence for NMR Fourier imaging applications, *J. Magn. Reson.* **69**, 488 (1986).
- [21] A. M. Souza, G. A. Álvarez, and D. Suter, Robust Dynamical Decoupling for Quantum Computing and Quantum Memory, *Phys. Rev. Lett.* **106**, 240501 (2011).
- [22] Z.-Y. Wang and R.-B. Liu, Protection of quantum systems by nested dynamical decoupling, *Phys. Rev. A* **83**, 022306 (2011).
- [23] S. Kotler, N. Akerman, Y. Glickman, A. Keselman, and R. Ozeri, Single-ion quantum lock-in amplifier, *Nature (London)* **473**, 61 (2011).
- [24] A. M. Souza, G. A. Álvarez, and D. Suter, Robust dynamical decoupling, *Phil. Trans. R. Soc. A* **370**, 4748 (2012).
- [25] Ł. Cywiński, R. M. Lutchyn, C. P. Nave, and S. Das Sarma, How to enhance dephasing time in superconducting qubits, *Phys. Rev. B* **77**, 174509 (2008).
- [26] G. S. Uhrig, Exact results on dynamical decoupling by π pulses in quantum information processes, *New J. Phys.* **10**, 083024 (2008).
- [27] G. S. Uhrig, Keeping a Quantum Bit Alive by Optimized π -Pulse Sequences, *Phys. Rev. Lett.* **98**, 100504 (2007).
- [28] G. de Lange, Z. H. Wang, D. Ristè, V. V. Dobrovitski, and R. Hanson, Universal dynamical decoupling of a single solid-state spin from a spin bath, *Science* **330**, 60 (2010).
- [29] C. A. Ryan, J. S. Hodges, and D. G. Cory, Robust Decoupling Techniques to Extend Quantum Coherence in Diamond, *Phys. Rev. Lett.* **105**, 200402 (2010).
- [30] B. Naydenov, F. Dolde, L. T. Hall, C. Shin, H. Fedder, L. C. L. Hollenberg, F. Jelezko, and J. Wrachtrup, Dynamical decoupling of a single-electron spin at room temperature, *Phys. Rev. B* **83**, 081201(R) (2011).
- [31] A. Rotem, T. Gefen, S. Oviedo-Casado, J. Prior, S. Schmitt, Y. Burak, L. McGuinness, F. Jelezko, and A. Retzker, Limits on Spectral Resolution Measurements by Quantum Probes, *Phys. Rev. Lett.* **122**, 060503 (2019).
- [32] J. Casanova, Z.-Y. Wang, J. F. Haase, and M. B. Plenio, Robust dynamical decoupling sequences for individual-nuclear-spin addressing, *Phys. Rev. A* **92**, 042304 (2015).
- [33] M. H. Abobeih, J. Cramer, M. A. Bakker, N. Kalb, M. Markham, D. J. Twitchen, and T. H. Taminiau, One-second coherence for a single electron spin coupled to a multi-qubit nuclear-spin environment, *Nat. Commun.* **9**, 2552 (2018).
- [34] Z.-Y. Wang, J. E. Lang, S. Schmitt, J. Lang, J. Casanova, L. McGuinness, T. S. Monteiro, F. Jelezko, and M. B. Plenio, Randomization of Pulse Phases for Unambiguous and Robust Quantum Sensing, *Phys. Rev. Lett.* **122**, 200403 (2019).
- [35] P. London, P. Balasubramanian, B. Naydenov, L. P. McGuinness, and F. Jelezko, Strong driving of a single spin using arbitrarily polarized fields, *Phys. Rev. A* **90**, 012302 (2014).
- [36] F. Reinhard, F. Shi, N. Zhao, F. Rempp, B. Naydenov, J. Meijer, L. T. Hall, L. Hollenberg, J. Du, R.-B. Liu, and J. Wrachtrup, Tuning a Spin Bath through the Quantum-Classical Transition, *Phys. Rev. Lett.* **108**, 200402 (2012).
- [37] E. Bauch, C. A. Hart, J. M. Schloss, M. J. Turner, J. F. Barry, P. Kehayias, S. Singh, and R. L. Walsworth, Ultralong Dephasing Times in Solid-State Spin Ensembles via Quantum Control, *Phys. Rev. X* **8**, 031025 (2018).
- [38] S. Schmitt, T. Gefen, F. M. Stürner, T. Uden, G. Wolff, C. Müller, J. Scheuer, B. Naydenov, M. Markham, S. Pezzagna, J. Meijer, I. Schwarz, M. Plenio, A. Retzker, L. P. McGuinness, and F. Jelezko, Submillihertz magnetic spectroscopy performed with a nanoscale quantum sensor, *Science* **356**, 832 (2017).
- [39] A. Ajoy, X. Lv, E. Druga, K. Liu, B. Safvati, A. Morabe, M. Fenton, R. Nazaryan, S. Patel, T. F. Sjolander, J. A. Reimer, D. Sakellariou, C. A. Meriles, and A. Pines, Wide dynamic range magnetic field cyclers: Harnessing quantum control at low and high fields, *Rev. Sci. Instrum.* **90**, 013112 (2019).
- [40] H. Zheng, J. Xu, G. Z. Iwata, T. Lenz, J. Michl, B. Yavkin, K. Nakamura, H. Sumiya, T. Ohshima, J. Isoya, J. Wrachtrup, A. Wickenbrock, and D. Budker, Zero-Field Magnetometry Based on Nitrogen-Vacancy Ensembles in Diamond, *Phys. Rev. Applied* **11**, 064068 (2019).
- [41] J. F. Barry, J. M. Schloss, E. Bauch, M. J. Turner, C. A. Hart, L. M. Pham, and R. L. Walsworth, Sensitivity optimization for NV-diamond magnetometry, *Rev. Mod. Phys.* **92**, 015004 (2020).
- [42] J. Cerrillo, A. Retzker, and M. B. Plenio, Fast and Robust Laser Cooling of Trapped Systems, *Phys. Rev. Lett.* **104**, 043003 (2010).
- [43] J. Cerrillo, A. Retzker, and M. B. Plenio, Double-path dark-state laser cooling in a three-level system, *Phys. Rev. A* **98**, 013423 (2018).
- [44] K. Fang, V. M. Acosta, C. Santori, Z. Huang, K. M. Itoh, H. Watanabe, S. Shikata, and R. G. Beausoleil, High-Sensitivity Magnetometry Based on Quantum Beats in Diamond Nitrogen-Vacancy Centers, *Phys. Rev. Lett.* **110**, 130802 (2013).
- [45] H. J. Mamin, M. H. Sherwood, M. Kim, C. T. Rettner, K. Ohno, D. D. Awschalom, and D. Rugar, Multipulse Double-Quantum Magnetometry with Near-Surface Nitrogen-Vacancy Centers, *Phys. Rev. Lett.* **113**, 030803 (2014).
- [46] C. Munuera-Javaloy, I. Arrazola, E. Solano, and J. Casanova, Double quantum magnetometry at large static magnetic fields, *Phys. Rev. B* **101**, 104411 (2020).
- [47] M. J. Biercuk, H. Uys, A. P. VanDevender, N. Shiga, W. M. Itano, and J. J. Bollinger, Experimental Uhrig dynamical

decoupling using trapped ions, *Phys. Rev. A* **79**, 062324 (2009).

- [48] T. Ishikawa, A. Yoshizawa, Y. Mawatari, H. Watanabe, and S. Kashiwaya, Influence of Dynamical Decoupling Sequences with Finite-Width Pulses on Quantum Sensing for AC Magnetometry, *Phys. Rev. Applied* **10**, 054059 (2018).
- [49] See Supplemental Material at <http://link.aps.org/supplemental/10.1103/PhysRevLett.126.220402> for analytic derivation of the two-level filter function, comparison to double quantum method, numerical Hahn-echo filter functions, relationship between filter functions, coherence times and sensitivity, and robustness to pulse errors.